Gold nanoparticle synthesis in worm-like catanionic micelles: microstructure conservation and temperature induced recovery†

Benjamin Abécassis,*[a] Fabienne Testard[a] and Thomas Zemb[ab]

Received 22nd September 2008, Accepted 31st October 2008
First published as an Advance Article on the web 17th December 2008
DOI: 10.1039/b816427d

Spherical gold nanoparticles are synthesized in worm-like catanionic reverse micelles, demonstrating the absence of shape templating except when the growth of the particles is slow. *In situ* time resolved SAXS measurements show that the microstructure of the microemulsion is conserved during the whole reaction. The liquid–liquid phase transition of the catanionic microemulsion induced by a gentle cooling is used to recover and purify the nanoparticles in a simple manner.

1 Introduction

Among various synthesis procedures, the use of reverse micelles is an effective route for yielding a wide range of nanoparticles of different chemical nature, size and shape.[1] The inner core of the reverse micelles acts as a nanoreactor and the nanoparticles are obtained by mixing two microemulsions containing reacting precursors. Despite numerous theoretical studies[2] on the formation mechanism of nanoparticles in reverse microemulsion, its elucidation is still far from being complete. Linking the size and shape of nanoparticles obtained at the end of the reaction to the shape and curvature radius of the microemulsion initially present is tempting but other parameters can also play an important role.[3] For example, the state of the water molecules inside the water pools, the dynamics of the inter droplet exchange, and the chemical conditions are of primary importance and can prevail over the templating effect.[3] As a matter of fact, when using spherical reverse micelles, the control of the nanoparticles' final radius by the content of the water droplet is not a general rule.[1] Templating effect should also be considered with precaution since atoms in a given nanoparticle were initially spanned in typically 10^3 micelles. Claims that using anisotropic reverse micelles can yield rod-shaped nanoparticles from a templating effect independently of other parameters[4] are to be taken with care since the microstructure of the microemulsion used is not elucidated initially nor during the growth of nanoparticles.

The recovery of the nanoparticles and their separation from unreacted species and excess surfactant is still a key step when using reverse micelles. Separation can be obtained with classical techniques such as ultracentrifugation,[5] solvent evaporation[6] or addition of a suitable solvent to cause phase separation or precipitation.[7] Very few methods using the properties of the surfactant are described in the literature. The thermoreversible properties of block copolymer surfactants can be used to induce a phase separation.[8] More recently, a light-induced flocculation is obtained with photodestructible surfactants.[9]

Here, we use a reverse microemulsion based on catanionic surfactants[10] to synthesize and recover gold nanoparticles using a temperature induced phase separation resulting from the catanionic properties. Original nano-structures were obtained by other groups using similar surfactants[11] but the role of the catanionic system was not elucidated.

2 Experimental

2.1 Chemicals

Octanoic acid (99.5%), octylamine (99%), octane (99%), gold hydrochloride, sodium borohydride are purchased from Sigma-Aldrich. The catanionic surfactant is obtained by mixing equal quantities of octanoic acid and octylamine in diethylether followed by evaporation of the solvent under vacuum which finally gives a white powder as described in ref. 12. Deionised water from a Milli-Q purification system (Millipore, USA) of resistivity 18.2 MΩ cm is used in preparing samples.

2.2 Sample preparation

To prepare a microemulsion, given quantities of octane, catanionic surfactant (0.8 M in the final solution), and an aqueous solution containing either gold hydrochloride (0.1 M) or sodium borohydride (0.1 M), are weighted in a teflon screw cap vial and vortex mixed. A clear, low viscous solution is obtained. We call R_w the ratio between the water and surfactant concentration, h the ratio between the borohydride and gold concentration. In the present study, the gold concentration in the final solution is 1.4×10^{-3} M. The gold nanoparticles are obtained by quickly mixing the two microemulsions under magnetic agitation. The solution, which is initially faint yellow, turns into red within 1 s showing the actual presence of gold nanoparticles.

2.3 TEM and UV-visible spectroscopy

Transmission electron microscopy (TEM) was performed on a Philips CM12 operated at 80 kV, on carbon-coated copper grids.

[a]*CEA, IRAMIS, SCM, LIONS, F-91191 Gif-sur-Yvette, France. E-mail: benjamin.abecassis@gmail.com; fabienne.testard@cea.fr*
[b]*Institut de Chimie Séparative de Marcoule, UMR5257, CEA/CNRS/UM2.ENSCM, BP 17171, 30207 Bagnols Sur Ceze. E-mail: thomas.zemb@icsm.fr*

† Electronic supplementary information (ESI) available: TEM images of gold nanoparticles. See DOI: 10.1039/b816427d

The UV-visible spectra were recorded using a deuterium/tungsten light and a J and M Diode array detector equiped with 256 diodes. The acquisition time was 0.8 ms.

2.4 SAXS

SAXS patterns were recorded at the ESRF (European Synchrotron Radiation Facility, Grenoble, France) on the high brilliance ID-2 beamline with the experimental conditions described in ref. 14. For our experiments, the wavelength was set to 1.1 Å (11.5 keV) to avoid the absorption edge of gold (11.92 keV). With a sample to detector distance of 1.5 m, the q-range spans from 0.15 nm^{-1} to 3.7 nm^{-1}. A FReLON (Fast-Readout, Low Noise) CCD camera developed by the ESRF was used to obtain high spatial and time resolutions. An optimised acquisition time of 50 ms was chosen for our experiments with a minimal read out pause of 80 ms between two acquisitions. The acquisition set-up is synchronised with the stopped-flow apparatus

2.5 Stopped-flow

We used a stopped-flow device SFM-400 from Biologic to enable fast turbulent mixing of the precursor solutions through a mixing chamber. The reaction solutions were injected in the analysis cell and immobilized by a hard-stop system (Biologic) to avoid overpressure artifacts and ensure steadiness during the acquisition. For UV-visible experiments a quartz transmittance cuvette (1.5 mm thickness, FC-15 biologic) was used. For SAXS experiments, a dedicated observation cell was set up to include a quartz capillary of 1.5 mm thickness (Glass tecknic). In a typical sequence, 300 µl of each solution were mixed without acquisition to fill the delay lines, after 5 ms, 100 µl of each solution are mixed and synchronized with the detection (UV or SAXS). After an experiment, the cell of the stopped-flow was washed using the experimental procedure described in ref. 14.

3 Results and discussion

Recently, we investigated in detail the structure of reverse microemulsions made of water, octane and octylamine-octanoic acid catanionic surfactant.[12] Depending on the water content, the temperature and surfactant concentration, several topologies can prevail, including spherical, rodlike or worm-like micelles. The shape adopted results from a compromise between the curvature imposed by the water to surfactant ratio and the spontaneous curvature related to the lateral interaction between charged head-groups. Spherical micelles are first observed in the surfactant–octane binary mixture with a very small amount of water. Adding more water results in the elongation of the micelles, leading to cylinders and worm-like micelles which eventually become connected. The density of connections between cylinders depends on the spontaneous curvature of the surfactant film (counted positive towards the water phase): low spontaneous curvature favours the saddle structure of junctions whereas end-caps are preferred for high spontaneous curvature. In this catanionic system, the spontaneous curvature can be tuned by the temperature. Upon cooling, the spontaneous curvature decreases, inducing a multiplication of junctions. When the effective attractive force caused by the junctions overcomes the entropy of mixing, a liquid–liquid phase separation occurs with the supernatant being almost pure oil, poor in surfactant and water.[12] This re-entrant phase separation will be used to recover the nanoparticles.

Fig. 1 shows TEM pictures of the nanoparticles obtained for different R_w and h values. For $h = 10$, the water to surfactant ratio impacts the polydispersity of the nanoparticle distribution

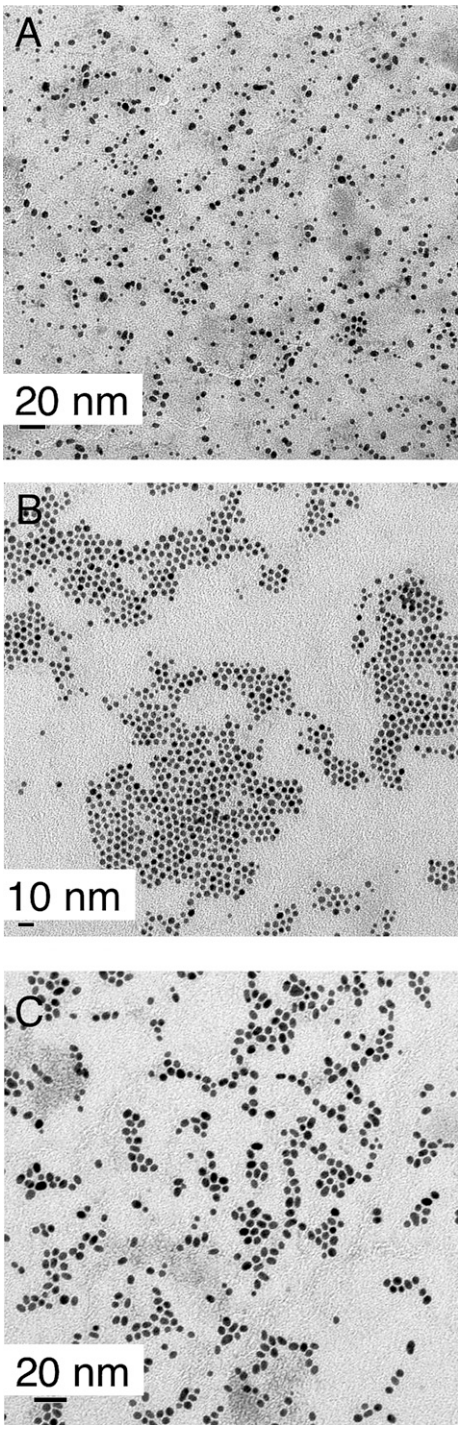

Fig. 1 TEM micrographs of the gold nanoparticles for different experimental conditions: (A) $R_w = 1$, $h = 10$; (B) $R_w = 2$, $h = 10$; (C) $R_w = 2$, $h = 5$. Larger views are available in the ESI.†

as evidenced by the comparison between Fig. 1A and 1B. $R_w = 2$ yields monodisperse spherical particles of around 8 nm in diameter (Fig. 1B) while polydispersed spherical particles are obtained when $R_w = 1$ (Fig. 1A). We have previously shown[12] that the microemulsion adopts a large anisotropic shape in this composition range with an increase in the length of the rodlike micelles when R_w increases from 1 to 2. Thus, the template's topology does not influence the nanoparticle's shape. For $R_w = 2$, decreasing the quantity of reducing agent, all other parameters being equal, makes the reaction slower (as evidenced by visual observation of the colour change) and induces a (small) anisotropy of the gold nanoparticles. The close examination of Fig. 1C reveals that for $h = 5$ the particles are slightly elliptical, the ellipticity (defined as the ratio between the large and the small dimensions) being of the order of 1.3.

Time resolved small angle X-ray scattering (SAXS) and UV-visible spectroscopy can give some information on both the formation of the nanoparticles and the structure of the microemulsion during the reaction.[13] We use a stopped-flow device coupled to the high flux available on the high resolution ID02 beam line at the ESRF and UV-visible spectrophotometer as described in ref. 14 for a single phase gold synthesis. UV-visible spectra (Fig. 2) show the continuous formation of the nanoparticles with the increasing intensity of the plasmon peak at 510 nm. No break is seen in the maximum absorbance plotted against time curve, suggesting that nucleation and growth are not separated in this case.[14] Fig. 3 shows two SAXS patterns obtained after 0.136 s and 15.476 s after the mixing of the two solutions. At 0.136 s, in the low-q part of the SAXS diagram, the intensity scales like $q^{1.3}$ while no gold particles are detected by UV-visible spectroscopy. This corresponds to a fractal structure of interconnected long wormlike micelles as previously shown by neutron scattering for the same microemulsion composition.[12]

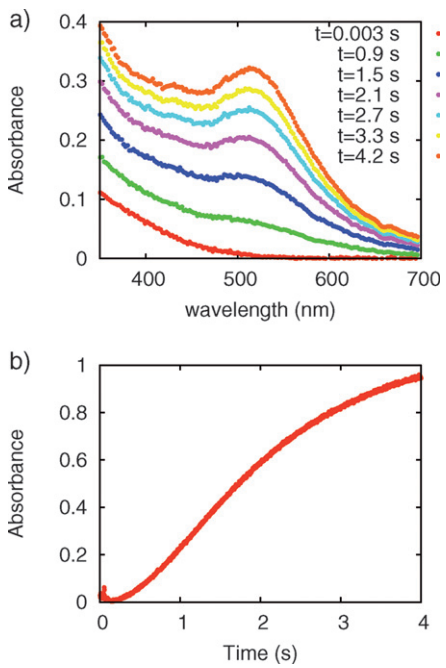

Fig. 2 (a) UV-visible spectra for several times during the reaction ($R_w = 2$, $h = 10$). (b) Plasmon intensity at 510 nm as a function of time.

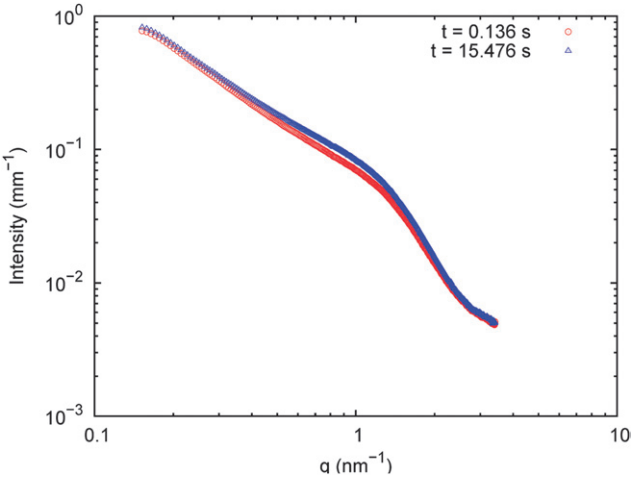

Fig. 3 SAXS patterns of the microemulsion solution during the nucleation and growth of gold nanoparticles, 0.136 s and 15.476 s after mixing of the two precursor solutions. The experimental conditions are $h = 10$ and $R_w = 2$.

After the nanoparticle formation, the scattered intensity remains unchanged in the low-q part of the SAXS diagram and is slightly higher in the intermediate q-range. The low total concentration of gold (1.4×10^{-3} M) is responsible for this very small excess scattering. The scattered intensity is dominated by the microemulsion's signal and a complete treatment of the nucleation and growth of gold nanoparticles as given in ref. 14 is not possible here due to low signal to noise ratio for gold nanoparticle. Assuming a complete conversion of molecular gold into nanoparticles we roughly estimate the scattered intensity due the nanoparticles to be 0.59 mm^{-1}, which is the correct order of magnitude. We can conclude from the very low modification of the SAXS patterns that the structure of the microemulsion is preserved throughout the nanoparticle synthesis.

These experiments, together with the TEM analysis show that the templating effect is not universal in the synthesis of nanoparticles in microemulsion. Gold spherical particles are obtained from wormlike reverse micelles and the structure of the microemulsion is preserved during the reaction. With a simple geometrical model of the microemulsion we can calculate the total length of micelle necessary to yield one nanoparticle. A spherical gold nanoparticle of 8 nm in diameter is composed of around 16 000 gold atoms. Considering our salt concentrations and the dimensions of the micelles determined in our previous study, this means that the monomers are initially spanned over a contour length of 2.7×10^5 nm, three orders of magnitude larger than one micelle. A more quantitative view of the formation mechanism is a demanding task as the dynamic of the complex microemulsion network has to be coupled to the nucleation and growth of the nanoparticles. This spans out of the scope of the present manuscript. We have to point out the importance of both the microemulsion structure and the specific chemistry of the nanoparticle formation. Shi *et al.*[11] have obtained in a similar microemulsion nanoparticles mimicking the connected wormlike structure of a catanionic microemulsion. Our results show that with the same template structure, changing the chemistry (gold reduction instead of insoluble oxide precipitation) can have a dramatic effect on the final shape of the nano particles.

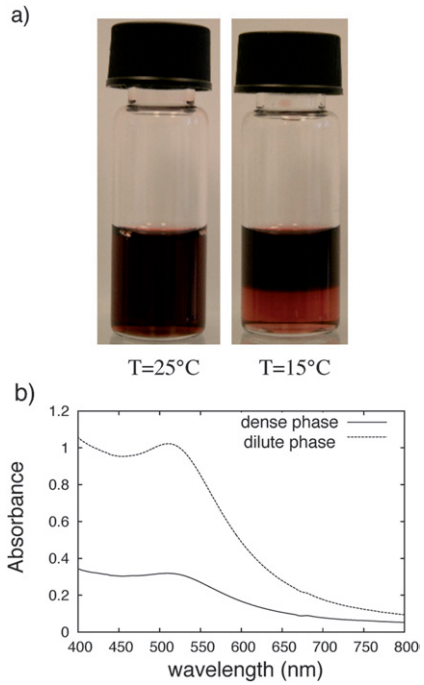

Fig. 4 (a) Photographs of the samples for two different temperatures above and below the liquid–liquid transition. (b) UV-visible spectra of the two phases after phase separation.

Finally, we use the conservation of the microstructure of the microemulsion during the formation of the nanoparticles to separate the nanoparticles from the rest of the solution. As already pointed out,[12] upon decreasing the temperature, the single phase microemulsion separates into a concentrated phase containing almost all the water and surfactant and a dilute phase composed of almost pure octane. This liquid–liquid transition is retained when gold nanoparticles are synthesised within the microemulsion. As shown in Fig. 4A, at 25 °C, the gold nanoparticles and the microemulsion co-exist in a single phase solution after the reaction. When the solution is gently cooled with a cold water bath, the solution phase separates at around 18 °C. The gold nanoparticles do not partition equally in the two phases: visual inspection of the demixed sample shows that the concentration in gold particles is higher in the dilute (top) phase than in the concentrated (bottom) phase. This is confirmed by the UV-visible spectra (Fig. 4B) where a 3.2 fold increase of the plasmon intensity is observed between the two solutions. Elementary analysis shows that the nitrogen and boron concentrations are ~11 times higher in the bottom than in the top phase indicating the presence of an excess of surfactant and by-products of the reaction in the bottom phase. After phase separation, we are thus facing a pure phase of octane in which most of the nanoparticles are dispersed by a small quantity of surfactant in equilibrium with a concentrated microemulsion containing the rest of the surfactant, water and the reaction by-products. By this means, the gold nanoparticles are separated and purified from the rest of the reaction mixture. That such a straightforward procedure can achieve these tasks is remarkable. Compared to other classical separation procedures this temperature induced purification has the advantage of preventing unwanted aggregation of the nanoparticles as indicated by the preserved plasmon band. This procedure could also be applied to nanoparticles obtained by different chemical routes. A pure catanionic microemulsion can be added to a raw nanoparticle dispersion and the subsequent decrease of temperature will lead to the purification of the nanoparticles. This could for example, be used in thermolysis synthesis of nanoparticles,[15] preventing numerous and lengthy precipitation–centrifugation cycles.

4 Conclusion

To conclude, we showed in a specific case that gold spherical nanoparticles are obtained whereas elongated wormlike micelles are used as template. The structure of the microemulsion is preserved during the reaction and the original temperature induced phase transition of the catanionic microemulsion can be used to separate the nanoparticles from the reaction by-products. We believe this behaviour to be a general, simple and efficient separation method for microemulsions showing a liquid–liquid phase transition in the ternary phase prism. These systems thus provide an interesting and potentially useful recovery method for nanoparticles.

Acknowledgements

We thank Jean Marc Verbavatz (DBCM/DSV, CEA Saclay) for the TEM characterization, ESRF (European Synhcrotron Radiation Facility, Grenoble, France) for provision of the beam time and Stéphanie Finet for help during the synchrotron experiments on the ID2 beamline.

References

1 M. P. Pileni, *J. Phys. Chem.*, 1993, **97**, 6961–6973; C. Petit, P. Lixon and M. Pileni, *J. Phys. Chem.*, 1993, **97**, 12974–12983; K. Holmberg, *J. Colloid Interface Sci.*, 2004, **274**, 355–364.
2 M. A. Lopez-Quintela, *Curr. Opin. Colloid Interface Sci.*, 2003, **8**, 137–144; M. Ethayaraja and R. Bandyopadhyaya, *J. Am. Chem. Soc.*, 2006, **128**, 17102–17113.
3 M. P. Pileni, *Nat. Mater.*, 2003, **2**, 145–150.
4 B. A. Simmons, S. C. Li, V. T. John, G. L. McPherson, A. Bose, W. L. Zhou and J. B. He, *Nano Lett.*, 2002, **2**, 263–268; Y. Song, R. M. Garcia, R. M. Dorin, H. R. Wang, Y. Qiu, E. N. Coker, W. A. Steen, J. E. Miller and J. A. Shelnutt, *Nano Lett.*, 2007, **7**, 3650–3655.
5 M. Duta, P. K. abd Jakupca, K. Reddy and N. Salvati, *Nature*, 1995, **374**, 44–46.
6 M. L. Steigerwald, A. P. Alivisatos, J. M. Gibson, T. D. Harris, R. Kortan, A. J. Muller, A. M. Thayer, T. M. Duncan, D. C. Douglass and L. E. Brus, *J. Am. Chem. Soc.*, 1988, **110**, 3046–3050.
7 D. H. Chen and S. H. Wu, *Chem. Mater.*, 2000, **12**, 1354–1360.
8 R. Zhang, J. Liu, B. X. Han, J. He, Z. M. Liu and J. L. Zhang, *Langmuir*, 2003, **19**, 8611–8614.
9 A. Vesperinas, J. Eastoe, S. Jackson and P. Wyatt, *Chem. Commun.*, 2007, 3912–3914.
10 T. Zemb, M. Dubois, B. Deme and T. Gulik-Krzywicki, *Science*, 1999, **283**, 816–819; M. Dubois, B. Deme, T. Gulik-Krzywicki, J. C. Dedieu, C. Vautrin, S. Desert, E. Perez and T. Zemb, *Nature*, 2001, **411**, 672–675; T. Zemb and M. Dubois, *Aust. J. Chem.*, 2003, **56**, 971–979; M. A. Hartmann, R. Weinkamer, T. Zemb, F. D. Fischer and P. Fratzl, *Phys. Rev. Lett.*, 2006, **97**, 018106.
11 H. T. Shi, L. M. Qi, J. M. Ma and H. M. Cheng, *Chem. Commun.*, 2002, 1704–1705; H. T. Shi, L. M. Qi, J. M. Ma, H. M. Cheng and B. Y. Zhu, *Adv. Mater.*, 2003, **15**, 1647; H. T. Shi, L. M. Qi, J. M. Ma and N. Z. Wu, *Adv. Func. Mat.*, 2005, **15**, 442–450; H. T. Shi, X. H. Wang, N. N. Zhao, L. M. Qi and J. M. Ma,

J. Phys. Chem. B., 2006, **110**, 748–753; H. Zhang, H. F. Li, D. Q. Li and S. L. Meng, *J. Colloid Interface Sci.*, 2006, **302**, 509–515.
12 B. Abecassis, F. Testard, L. Arleth, S. Hansen, I. Grillo and T. Zemb, *Langmuir*, 2006, **22**, 8017–8028; B. Abecassis, F. Testard, L. Arleth, S. Hansen, I. Grillo and T. Zemb, *Langmuir*, 2007, **23**, 9983–9989.
13 M. Andersson, J. S. Pedersen and A. E. C. Palmqvist, *Langmuir*, 2005, **21**, 11387–11396; P. Riello, M. Mattiazzi, J. S. Pedersen and A. Benedetti, *Langmuir*, 2008, **24**, 5225–5228.
14 B. Abecassis, F. Testard, O. Spalla and P. Barboux, *Nano Lett.*, 2007, **7**, 1723–1727.
15 Y. Yin and P. Alivisatos, *Nature*, 2005, **437**, 664–670.

